arXiv:1207.3963v1 [cond-mat.quant-gas] 17 Jul 2012

Density-induced processes in quantum gas mixtures in optical lattices

Ole Jürgensen, Klaus Sengstock, and Dirk-Sören Lühmann
Institut für Laser-Physik, Universität Hamburg, Luruper Chaussee 149, 22761 Hamburg, Germany

We show that off-site processes and multi-orbital physics have a crucial impact on the phase diagram of quantum gas mixtures in optical lattices. In particular, we discuss Bose-Fermi mixtures where the intra- and interspecies interactions induce competing density-induced hopping processes, the so-called bond-charge interactions. Furthermore, higher bands strongly influence tunneling and on-site interactions. We apply a multi-orbital interaction-induced dressing of the lowest band which leads to renormalized hopping processes. These corrections give rise to an extended Hubbard model with intrinsically occupation-dependent parameters. The resulting decrease of the tunneling competes with a decrease of the total on-site interaction energy both affecting the critical lattice depth of the superfluid to Mott insulator transition. In contrast to the standard Bose-Fermi-Hubbard model, we predict a large shift of the transition to shallower lattice depths with increasing Bose-Fermi attraction. The applied theoretical model allows an accurate prediction of the modified tunneling amplitudes and the critical lattice depth both recently observed experimentally.

PACS numbers: 03.75.Lm, 67.85.Pq, 71.10.Fd

Quantum gas mixtures in optical lattices are well suited to study in detail interaction-induced effects in condensed matter. They allow for the investigation of systems with spin degree of freedom and with different species of particles that can even obey different quantum statistics. In particular, the experimental realization of atomic mixtures of bosonic and fermionic particles (e.g., ^{87}Rb-^{40}K) in optical lattices [1–4] triggered a vivid discussion on the role of inter- and intraspecies interactions. These experiments allow for the observation of the bosonic superfluid to Mott-insulator transition in the presence of fermionic atoms. The prominent feature observed in all experiments is the decay of visibility and condensate fraction of the bosonic subsystem induced by the interaction with the fermionic atoms. Two possible explanations for this drop in bosonic coherence were proposed. First, the process of adiabatic heating while ramping the lattice has been suggested [5, 6]. It is caused by different contributions of the atomic species to the total entropy and is therefore specific to the loading procedure of experiments with ultracold gases. Second, an interaction-induced dressing of tunneling and interaction processes has been found that causes a shift of the superfluid to Mott-insulator phase transition[3, 7–9]. The latter effect corresponds to a necessary extension of the Hubbard model at zero temperature and is therefore fundamental for various lattice systems. The important role of interaction-induced processes in optical lattices is caused by the specific shape of the Wannier functions and the possibility of high filling factors.

The *standard* Bose-Fermi-Hubbard model [10] is restricted to the lowest single-particle band and on-site interactions. Interestingly, it fails to describe interaction effects in boson-fermion mixtures. Assuming a fermionic band-insulator, which is present in the experimental realizations [1–4], the boson-fermion interaction gives rise only to an irrelevant shift of the global chemical potential. Even for realistic assumptions for the confining potential, the interspecies interaction has little influence [11]. Due to an effective screening even a small shift in the opposite direction is predicted. In contrast to the experimental results, the superfluid phase is therefore more stable within this framework, which poses the question of the applicability of the standard Hubbard model in this case. It was pointed out that the Bose-Fermi-Hubbard parameters, i.e., tunneling and on-site interactions can be strongly influenced by the inclusion of higher orbitals and non-local interactions [7–9]. Off-site interactions include the so-called bond-charge interactions that have a direct density-dependent influence on the total tunneling [9, 12–18]. For purely bosonic systems and without taking off-site interactions into account, the inclusion of higher bands has been discussed in, e.g., Ref. [19–29]. Both extensions can be included in extended Hubbard models [9, 17, 18] and can be illustrated as effective modifications of the tunneling potentials for both atomic species [17].

Here, we present quantitative results for the phase diagram of Bose-Fermi mixtures using an extended Hubbard model with multi-orbitally dressed processes [17, 18]. It includes density-induced tunneling, so-called bond-charge interactions [9, 12–18], as well as a multi-orbitally renormalized tunneling and interaction processes [9, 17, 18, 27]. The physical effects discussed here are in general present for all interacting quantum gas mixtures. The exact results, however, depend on the quantum statistics of the particles and the specific parameters such as the detuning from the light potential and the atomic masses.

As a central result, we present the phase diagram of the superfluid to Mott-insulator transition in a Bose-Fermi mixture in section I. Furthermore, we discuss the crucial effect of off-site interactions and the corresponding shortcomings of the standard Bose-Fermi Hubbard model in section II. Subsequently, we present the procedure to incorporate higher-band processes in section III. Afterwards, the corresponding extended Hubbard models and the implications for the bosonic phase transition are discussed in detail in section IV.

I. PHASE DIAGRAMS

We will now first discuss the resulting phase diagrams of the bosonic superfluid to Mott-insulator transition in the presence of a fermionic band-insulator, where the individual cor-

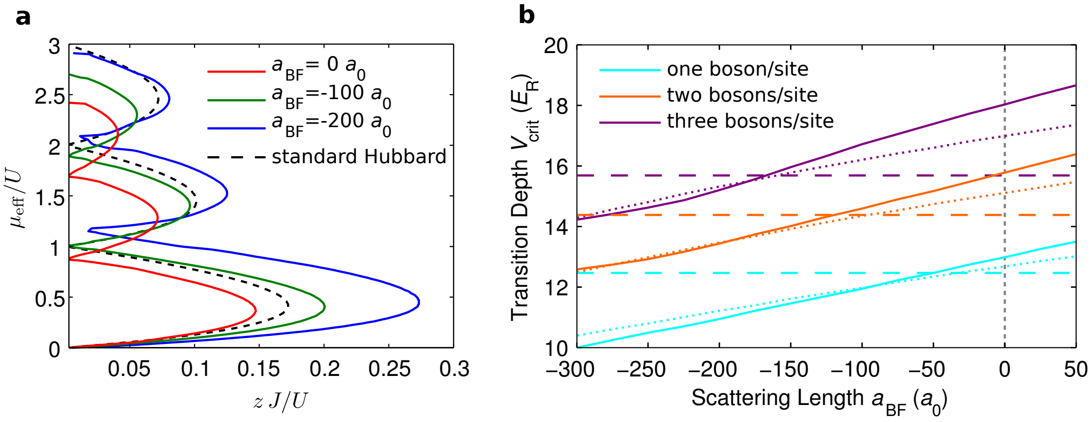

FIG. 1: **a** Phase diagram for the superfluid to Mott-insulator transition of bosons with a fermionic band-insulator at different interspecies attractions. The predictions of the standard Hubbard models are shown as a dahed black line. The attractive interaction effectively reduces the total tunneling resulting in extended Mott-lobes. **b** The critical lattice depth of the superfluid to Mott-insulator transition as a function of the interspecies scattering length $a_{\rm BF}$. The transition occurs at significantly shallower lattices than in the purely bosonic system ($a_{\rm BF}=0$). The dashed lines correspond to the Bose-Fermi Hubbard model and the dotted lines to an extended model with only lowest-band processes (section IV).

rections to the standard Hubbard model are discussed in detail below. For concreteness, we choose a mixture of bosonic ^{87}Rb and fermionic ^{40}K in an optical lattice with a spacing of $a=377\,$nm. For the respective wavelength, the Wannier functions of both species are almost identical. The interaction between the bosonic atoms is fixed to a repulsive scattering length of $a_{\rm BB}=102\,a_0$ [27], while the attractive interaction between the two species is tunable over a wide range using a Feshbach resonance [3]. The fermionic nature of the spin-polarized potassium atoms simplifies the system, as we can assume a band-insulating phase and thus a fixed atom-number of one fermion per lattice site. Note that it is possible to directly apply the presented methods and extensions to a variety of atomic quantum gas mixtures in lattices. In particular, both atomic species can be bosonic or fermionic and the generalization to multi-component systems with more than two species is straight forward.

For a fermionic band insulator, the fermionic degrees of freedom are frozen out and the physics can be described by an effective bosonic model that takes into account all effects induced by the interaction with the fermions. In the framework of this paper, we will discuss in detail the derivation of an effective Hamiltonian which reads

$$\tilde{H}_{\rm ext}=-\sum_{\langle i,j\rangle}\tilde{b}_i^\dagger\tilde{b}_j\tilde{J}^{\rm tot}_{\hat{n}_j,\hat{n}_i}+\sum_i\tilde{E}_{\hat{n}_i}-\mu\sum_i\hat{n}_i. \qquad (1)$$

We will see that despite its simplicity it already includes higher-band and bond-charge off-site processes. The latter gives rise to an occupation-dependent tunneling $J^{\rm tot}_{n_j,n_i}=J_{\rm B}+(n_i+n_j-1)X_{\rm BB}+2X_{\rm BF}$ even within the lowest single-particle band. Here, $J_{\rm B}$ is the conventional tunneling; $X_{\rm BB}$ and $X_{\rm BF}$ are the bond-charge tunneling elements arising from Bose-Bose and Bose-Fermi interactions, respectively (section II). The interaction induced occupation of higher orbitals leads to a further occupation dependency of all parameters, i.e., $\tilde{J}_{\rm B}$, $\tilde{X}_{\rm BB}$, $\tilde{X}_{\rm BF}$ and $\tilde{E}_n$.

The tilde above the parameters and operators in (1) indicates the multi-orbital dressing as discussed in section III. The effective single-band Hamiltonian (1) uses the ground state of the interacting system, called the dressed band, instead of the lowest single-particle band [17, 18]. The dressed operators $\tilde{b}_i$ and $\tilde{b}_i^\dagger$ annihilate and create bosonic particles on site i in this dressed band and $\hat{n}_i=\tilde{b}_i^\dagger\tilde{b}_i$ counts the number of bosons on site i. It is important to note that after the transformation to the dressed band, the phase diagrams can be calculated using standard single-band methods. The renormalized on-site energy $\tilde{E}_n$ is composed of the single particle energies of bosons $\tilde{\epsilon}_{{\rm B},n}$ and fermions $\tilde{\epsilon}_{{\rm F},n}$ as well as the interaction energies for the repulsion between the bosons $\frac{1}{2}n(n-1)\tilde{U}_n$ and the attraction between the species $n\tilde{U}_{{\rm BF},n}$. The chemical potential μ fixes the total number of bosonic atoms.

After calculating the dressed parameters, we apply Gutzwiller mean-field theory to compute the critical lattice depth of the transition from the superfluid to the Mott-insulator. The phase diagrams of the extended model (1) are shown in Fig. 1**a**. The effective chemical potential $\mu-\tilde{E}_1$ is given in units of the Hubbard on-site interaction U, where $\tilde{E}_1$ is the renormalized on-site energy of one boson and one fermion. For vanishing interaction between the bosons and fermions $a_{\rm BF}=0$ and a repulsive interaction $a_{\rm BB}=102\,a_0$ among the bosons, the Mott-lobes are contracted compared with the standard Hubbard model. This is a result of a decrease of the on-site energy and an increase of the total tunneling caused by off-site interactions [17]. For increasing attraction between bosons and fermions the effect is reversed [9] and the Mott-lobes are extended exhibiting a critical transition point at much lower lattice depths. This effect can be attributed to a strong reduction of the total tunneling amplitude induced by off-site interactions.

In Fig. 1**b** the critical lattice depths for the superfluid to Mott insulator transition for one, two and three bosons per lattice site are shown as a function of the interspecies interaction strength. The solid lines depict the results obtained using the extended model (1), while the dashed lines correspond to the standard Bose-Fermi Hubbard model, which predicts no dependency on the interspecies interaction a_{BF} (section II). As discussed above, for $a_{\mathrm{BF}} = 0$ the Mott-insulator transition is shifted to deeper lattices, where the shift is increased with the bosonic filling. This is mainly caused by the bosonic bond-charge interaction $\tilde{X}_{\mathrm{BB}}$ enhancing the total tunneling. With increasing attractive interaction a_{BF} the transition is strongly shifted to shallower lattice depths. Depending on the filling, the shift of the Mott-insulator transition caused by the fermionic atoms is 3-4 E_{R} for $a_{\mathrm{BF}} = -300\,a_0$.

The predicted shift is considerably larger than calculated with the adiabatic band elimination method in Ref. [9] which also incorporates the bond-charge interactions. The effective potential approach in Refs. [3, 7] does not include the important contributions of fermionic on-site energy and bosonic bond-charge interaction. The extended Bose-Fermi-Hubbard model (1) discussed here contains all relevant energies that can affect the superfluid to Mott-insulator transition at zero temperature. As a result, the Mott-insulator shift in Ref. [3] can be partly explained by interaction-induced effects. This provides a consistent picture, where the experimental observations [1–3] are a combined effect of the Hubbard extensions *and* the adiabatic heating processes [5, 6] which depend on the initial temperature of the quantum gas.

II. OFF-SITE INTERACTIONS

We now turn back to the full description of the applied extended Hubbard model which features two corrections to the standard Hubbard model. First, off-site interactions lead to a significant contribution to the total tunneling amplitude by changing the effective tunneling potential. Second, the inclusion of multi-band processes causes a modification of all model parameters.

As mentioned above, mixtures of ultracold spin-polarized bosonic and fermionic atoms in optical lattices are usually described by the standard Bose-Fermi Hubbard model. The underlying tight-binding approximation restricts the model to the lowest single-particle orbital and interactions between particles on the same lattice site. The resulting Hubbard Hamiltonian reads

$$\begin{aligned}\hat{H}_{\mathrm{BFH}} = &-\sum_{\langle i,j\rangle}(J_{\mathrm{B}}\hat{b}_i^\dagger\hat{b}_j + J_{\mathrm{F}}\hat{f}_i^\dagger\hat{f}_j) + \frac{U_{\mathrm{BB}}}{2}\sum_i \hat{n}_i(\hat{n}_i - 1)\\ &+ \sum_i U_{\mathrm{BF}}\hat{n}_i\hat{m}_i - \sum_i(\mu_{\mathrm{B}}\hat{n}_i + \mu_{\mathrm{F}}\hat{m}_i),\end{aligned} \tag{2}$$

Here, $\hat{b}_i$ ($\hat{f}_i$) is the bosonic (fermionic) annihilation operator and $\hat{n}_i$ ($\hat{m}_i$) the respective particle number operator. In general, the tunneling matrix elements for bosons (J_{B}) and fermions (J_{F}) can have different values. The on-site interaction is fully described by the parameters U_{BB} and U_{BF} for intra- and interspecies interaction, respectively. The total number of bosonic and fermionic atoms are fixed by the chemical potentials μ_{B} and μ_{F}. Under common experimental conditions [1–4], the fermions are in a band-insulator phase where Pauli-blocking prohibits tunneling. This freezes out the fermionic degrees of freedom and the resulting Hamiltonian captures the behavior of the bosons under the influence of exactly one fermion per lattice site. Consequently, we can set $\hat{f}_i^\dagger\hat{f}_j \to 0,\ \hat{m}_i \to 1$ and get

$$\begin{aligned}\hat{H}_{\mathrm{FBI}} = &-\sum_{\langle i,j\rangle} J_{\mathrm{B}}\hat{b}_i^\dagger\hat{b}_j + \frac{U_{\mathrm{BB}}}{2}\sum_i \hat{n}_i(\hat{n}_i - 1)\\ &+ \sum_i (U_{\mathrm{BF}} - \mu_{\mathrm{B}})\hat{n}_i.\end{aligned} \tag{3}$$

The interaction energy U_{BF} between bosons and fermions can be absorbed into an effective chemical potential $\mu_{\mathrm{eff}} = \mu_{\mathrm{B}} - U_{\mathrm{BF}}$ and the resulting Hamiltonian does not differ from the standard Bose-Hubbard model. Thus, the behavior of the bosons is not influenced by the homogeneously distributed fermions, which is in contradiction to the experimental observations [1–3].

In the derivation of the standard Hubbard model, it is argued that interaction processes between particles on neighboring lattice sites can be neglected due to their small amplitudes compared with on-site interactions. This argument is however only partly correct, since some of these processes, such as bond-charge interactions, involve the hopping of particles. Compared to the conventional tunneling, these processes can be non-negligible and consequently alter the phase diagrams. In particular, the Wannier functions in optical lattices differ strongly from their counterpart in solid state materials leading to comparably large matrix elements for bond-charge processes. In addition, the possibility of larger fillings in bosonic systems can enlarge these interaction effects. Consequently, off-site interaction processes can be strongly enhanced for optical lattice systems.

Consider the interacting part of the full two-particle Hamiltonian for the lowest band and two neighboring lattice sites L and R

$$\hat{H}_{\mathrm{int}} = \frac{1}{2}\sum_{ijkl} U_{ijkl}^{\mathrm{BB}}\,\hat{b}_i^\dagger\hat{b}_j^\dagger\hat{b}_k\hat{b}_l + \sum_{ijkl} U_{ijkl}^{\mathrm{BF}}\,\hat{b}_i^\dagger\hat{f}_j^\dagger\hat{f}_k\hat{b}_l, \tag{4}$$

with $i, j, k, l = \mathrm{L}, \mathrm{R}$ and

$$\begin{aligned}U_{ijkl}^{\mathrm{BB/BF}} &= g_{\mathrm{BB/BF}} \int\ w_i^{\mathrm{B}*}(\mathbf{r})\, w_j^{\mathrm{B/F}*}(\mathbf{r}')\, V(\mathbf{r},\mathbf{r}')\\ &\qquad\times w_k^{\mathrm{B/F}}(\mathbf{r}')\, w_l^{\mathrm{B}}(\mathbf{r})\ \ d^3r\, d^3r'.\end{aligned} \tag{5}$$

The basis functions $w_i^{\mathrm{B/F}}(\mathbf{r})$ are the maximally localized Wannier functions that describe a boson/fermion sitting on site i and the interaction strengths are given by $g_{\mathrm{BB}} = \frac{4\pi\hbar^2}{m_{\mathrm{B}}}a_{\mathrm{B}}$ and $g_{\mathrm{BF}} = \frac{2\pi\hbar^2}{m_{\mathrm{r}}}a_{\mathrm{BF}}$ with the mass of the bosonic atoms m_{B} and the reduced mass m_{r} of boson and fermion. The interaction potential $V(\mathbf{r},\mathbf{r}')$ we applied describes the scattering properties using a finite-ranged box potential (see [17]). In a lowest-band treatment, this is usually replaced by contact interactions, i.e., a δ-pseudopotential. In a multi-orbital framework the latter would lead to mathematical subtleties [25].

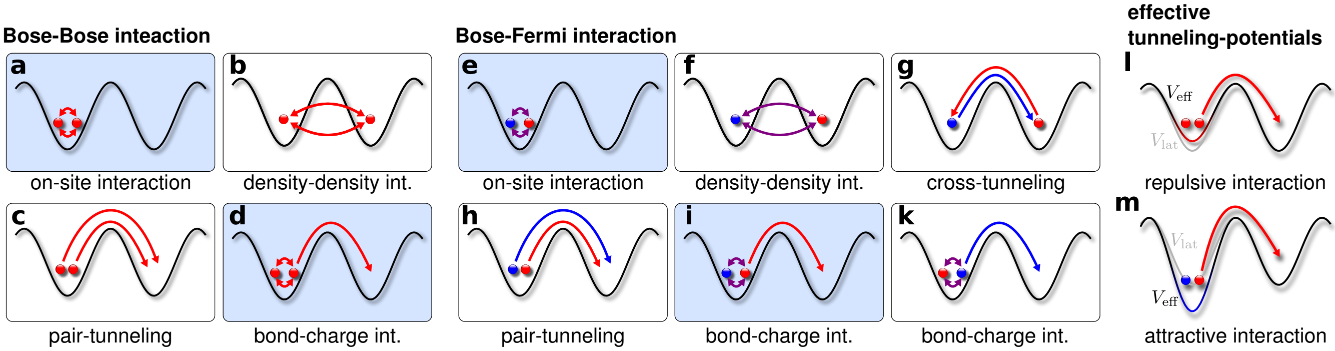

FIG. 2: Interaction-induced off-site processes. Processes induced by the Bose-Bose interaction are **a** bosonic on-site interaction, **b** density-density interaction, **c** pair-tunneling, and **d** bond-charge tunneling. Analogous interaction processes are induced by Bose-Fermi interaction, namely, **e** on-site interaction, **f** density-density-interaction, **g** cross-tunneling, **h** pair-tunneling, **i** bond-charge tunneling of a boson and **k** bond-charge tunneling of a fermion. The shading indicates the most important processes that are taken into account in the extended Hubbard model (1). The bond-charge tunneling processes (**d** and **i**) are illustrated in **l** and **m** via tunneling in effective potentials.

The distinct processes arising from the full two-body Hamiltonian (4) for Bose-Bose and the Bose-Fermi interaction are depicted in Fig. 2. In addition to the on-site interaction, the Bose-Bose interaction leads to the density-density interaction process $V_{\rm BB}\,\hat{n}_i\hat{n}_j$, the correlated tunneling of a particle pair $P_{\rm BB}\,\hat{b}_i^{\dagger 2}\hat{b}_j^2$, and the bond-charge assisted tunneling $-X_{\rm BB}\,\hat{b}_i^\dagger(\hat{n}_i+\hat{n}_j)\hat{b}_j$. The respective matrix elements are $V_{\rm BB}=U^{\rm BB}_{ijji}$, $P_{\rm BB}=U^{\rm BB}_{iijj}/2$, and $X_{\rm BB}=-U^{\rm BB}_{iiij}=-U^{\rm BB}_{ijjj}$. The amplitudes of these processes are plotted in Fig. 3 as solid lines. While the density-density interaction $V_{\rm BB}$ and the pair tunneling amplitude $P_{\rm BB}$ are several orders of magnitudes smaller than the the standard Hubbard processes, the bond-charge interaction $X_{\rm BB}$ is only one order of magnitude smaller than the conventional tunneling $J_{\rm B}$. As the bond-charge interaction $-X_{\rm BB}\,\hat{b}_i^\dagger(\hat{n}_i+\hat{n}_j)\hat{b}_j$ scales with the particle number on both involved sites, it can easily reach non-negligible values and must be accounted for (see also [17]). In addition, it scales linearly with the interaction strength which can be tuned experimentally. Here, it is essential that the bond-charge interaction contributes to the tunneling of the particles rather than the on-site interaction.

For the Bose-Fermi interaction two more processes exist as the interacting particles are distinguishable (Fig. 2b). First, the cross-tunneling, which is similar to the density-density interaction except that the particles interchange, and second, the bond-charge interaction, where either a bosonic or a fermionic particle tunnels. However, assuming a fermionic band insulator all processes involving the hopping of a fermion are forbidden. The respective amplitudes of the processes induced by Bose-Fermi interaction are plotted as dashed lines in Fig. 3.

In conclusion, only on-site interactions and bond-charge tunneling of bosons have to be taken into account (shaded in Fig. 2), since other processes are prohibited by the fermionic band-insulator or contribute only with extremely small amplitudes. Thus, the necessary extensions of the Hubbard Hamiltonian, i.e. the bond-charge processes in Fig. 2**d** and **i**, read

$$\hat{X}=\hat{X}_{\rm BB}+\hat{X}_{\rm BF}=\hat{b}_i^\dagger(U^{\rm BB}_{iiij}\hat{b}_i^\dagger\hat{b}_i+U^{\rm BB}_{ijjj}\hat{b}_j^\dagger\hat{b}_j +U^{\rm BF}_{iiij}\hat{f}_i^\dagger\hat{f}_i+U^{\rm BF}_{ijjj}\hat{f}_j^\dagger\hat{f}_j)\hat{b}_j. \qquad (6)$$

An intuitive physical understanding of the bond-charge tunneling induced by Bose-Bose as well as by Bose-Fermi interaction can be obtained by the analogy to an effective tunneling potential [17]. Assuming contact interactions in the single-band description and using the integral expressions (5), we can rewrite the expression (6) as

$$\hat{X}=\hat{b}_i^\dagger\hat{b}_j\int d^3r\;w_i^{\rm B*}(\mathbf{r})\left(g_{\rm BB}\hat{\rho}^{\rm BB}_{ij}+g_{\rm BF}\hat{\rho}^{\rm BF}_{ij}\right)w_j^{\rm B}(\mathbf{r}), \qquad (7)$$

where we introduced the reduced densities

$$\hat{\rho}^{\rm BB}_{ij}=\hat{n}_i|w_i^{\rm B}(\mathbf{r})|^2+(\hat{n}_j-1)|w_j^{\rm B}(\mathbf{r})|^2 \qquad (8)$$

$$\hat{\rho}^{\rm BF}_{ij}=\hat{m}_i|w_i^{\rm F}(\mathbf{r})|^2+\hat{m}_j|w_j^{\rm F}(\mathbf{r})|^2. \qquad (9)$$

The -1 in the bosonic density corresponds to the exclusion of self-interactions and is directly obtained from the commuta-

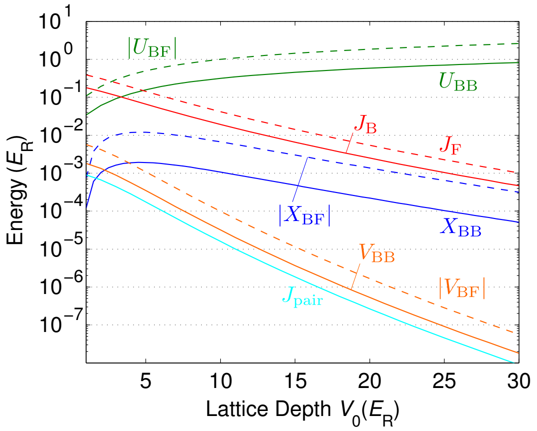

FIG. 3: Matrix elements for the different hopping and interaction processes. The solid lines are the purely bosonic processes, while the dashed lines correspond to Bose-Fermi interaction and fermionic tunneling. Shown are the intra- and interspecies on-site interaction $U_{\rm BB}$ and $U_{\rm BF}$ (green), the conventional tunneling amplitudes $J_{\rm B}$ and $J_{\rm F}$ (red), the bosonic bond-charge tunneling $X_{\rm BB}$ and $X_{\rm BF}$ (blue) as well as density-density interactions $V_{\rm BB}$ and $V_{\rm BF}$ (orange) and correlated pair-tunneling $P_{\rm BB}$ (cyan).

tion relations. Inside the integral, we can use the locality of the Wannier functions to replace these operators by the density functions $\hat{\rho}_{ij}^{\rm BB} \to \rho_{\rm B}(\mathbf{r}) - |w_j^{\rm B}(\mathbf{r})|^2$ and $\hat{\rho}_{ij}^{\rm BF} \to \rho_{\rm F}(\mathbf{r})$. The bond-charge tunneling operator (7) can now easily be unified with the conventional tunneling to find the expression

$$\hat{J} + \hat{X} = \langle w_i^{\rm B}(\mathbf{r})| \left(\frac{\mathbf{p}^2}{2m} + V_{\rm eff}(\mathbf{r}) \right) |w_j^{\rm B}(\mathbf{r})\rangle \, \hat{b}_i^\dagger \hat{b}_j \qquad (10)$$

which corresponds to the conventional tunneling in an effective potential $V_{\rm eff}(\mathbf{r}) = V(\mathbf{r}) + g_{\rm BB}(\rho_{\rm B}(\mathbf{r}) - |w_j^{\rm B}(\mathbf{r})|^2) + g_{\rm BF}\rho_{\rm F}(\mathbf{r})$.

In Fig. 2**k** and **l** the tunneling in effective potentials is sketched. Repulsive interactions, as between the bosons, effectively reduce the lattice depth, while attractive interactions have the opposite effect. Depending on the relative scattering lengths, the total tunneling can be strongly enhanced or reduced. This is consistent with the results for the fermionic tunneling obtained in [4]. The modification of the total tunneling in the lowest band already leads to a considerable deformation of the well-known phase diagram of the superfluid to Mott-insulator transition for bosons as discussed later in detail.

III. MULTI-ORBITAL RENORMALIZATION

Whereas in the previous section we introduced off-site interactions as an important extension to the standard Hubbard model, we will now discuss another important feature of the Hamiltonian (1), namely the effective inclusion of higher bands. In the standard Hubbard model approach, only the lowest single-particle band is assumed to be occupied. However, in the strongly correlated system particles are promoted to higher orbitals due to the interaction induced coupling between the bands. By changing their wave functions the particles minimize their on-site interaction energy (see section III.B). In particular, this also affects the tunneling and other off-site processes as outlined now in section III.A.

A. Multi-orbital dressing

For the following calculation of the multi-orbital effects, we assume the orbital occupation to be determined purely by on-site interactions, while off-site processes can be neglected due to the much smaller amplitudes. The problem can thus first be reduced to a single lattice site. The single-site ground state is a superposition of many-particle states $\Psi(n) = \sum_{N,M} c_{N,M} |N\rangle |M\rangle$. Here, $|N\rangle |M\rangle = |n_0, n_1, ...\rangle |m_0, m_1, ...\rangle$ is the product state with n_α bosons and m_α fermions in the Wannier orbital $w_{\rm B/F}^{(\alpha)}(\mathbf{r})$, where α indicates the orbital. The state $\Psi(n)$ consists of the lowest single-particle band dressed with small contributions of higher bands. At zero temperature the particles will exclusively occupy the dressed band $\Psi(n)$ instead of the lowest single-particle band.

In general, any multi-orbital two-site operator acting on sites L and R can be decomposed in operators of the form

$$\hat{O} = \sum_{\{\alpha\},\{\beta\}} A^{\{\alpha\},\{\beta\}} \hat{O}_{\rm L}^{\{\alpha\}} \hat{O}_{\rm R}^{\{\beta\}}, \qquad (11)$$

where the summation is over all possible sets of orbitals $\{\alpha\} = \{\alpha_1, \alpha_2, ...\}$ and $\{\beta\} = \{\beta_1, \beta_2, ...\}$. $A^{\{\alpha\},\{\beta\}}$ is the amplitude for the corresponding process and $\hat{O}_i^{\{\alpha\}}$ consists of creation and annihilation operators $\hat{b}_i^{(\alpha_k)\dagger}$ and $\hat{b}_i^{(\alpha_k)}$ for particles on site i in the orbital α_k. In the simplest case – the conventional tunneling from the right to the left site – we have only sets with a single orbital $\{\alpha\} = \alpha$ and $\{\beta\} = \beta$, the operators on the left and the right site $\hat{O}_{\rm L}^{\alpha} = \hat{b}_{\rm L}^{(\alpha)\dagger}$, $\hat{O}_{\rm R}^{\beta} = \hat{b}_{\rm R}^{(\beta)}$, and tunneling amplitudes $A^{\alpha,\beta}$ as defined below. Instead of collapsing this operator to the lowest single-particle band, we reduce it to the dressed band [17, 18] given by the many-particle ground state $\Psi(n)$. The effective operator $\tilde{O}$ in the dressed band takes the form

$$\tilde{O} = \tilde{A}_{n_{\rm L},n_{\rm R}} \tilde{O}_{\rm L} \tilde{O}_{\rm R}, \qquad (12)$$

where $\tilde{O}_i$ is obtained from $\hat{O}_i^{\{\alpha\}}$ by replacing all creation and annihilation operators $\hat{b}_i^{(\alpha_k)\dagger}$ and $\hat{b}_i^{(\alpha_k)}$ by their counterparts of the dressed band $\tilde{b}_i^\dagger$ and $\tilde{b}_i$. The operators of the dressed band fulfill the usual relations $\tilde{b}_i |\Psi(n)\rangle_i = \sqrt{n}\, |\Psi(n-1)\rangle_i$ and $\tilde{b}_i^\dagger |\Psi(n)\rangle_i = \sqrt{n+1}\, |\Psi(n+1)\rangle_i$.

The effective amplitude $\tilde{A}_{n_{\rm L},n_{\rm R}}$ is obtained from the matrix element $\langle \Psi_{\rm F}| \hat{O} |\Psi_{\rm I}\rangle$, where $\Psi_{\rm I}(n_{\rm L}, n_{\rm R})$ denotes the initial and $\Psi_{\rm F} = \Psi(n_{\rm L}', n_{\rm R}')$ the final state of the process. It thereby includes the summation over all multi-orbital processes. Since the states are product states of the individual lattice sites $|\Psi(n_{\rm L})\rangle |\Psi(n_{\rm R})\rangle$, also the effective amplitude $\tilde{A}$ decomposes into individual site contributions

$$\begin{aligned} \tilde{A}_{n_{\rm L},n_{\rm R}} = \frac{1}{N} \sum_{\{\alpha\},\{\beta\}} & A^{\{\alpha\},\{\beta\}} \langle \Psi(n_{\rm L}')| \hat{O}_{\rm L}^{\{\alpha\}} |\Psi(n_{\rm L})\rangle \\ & \times \langle \Psi(n_{\rm R}')| \hat{O}_{\rm R}^{\{\beta\}} |\Psi(n_{\rm R})\rangle, \end{aligned} \qquad (13)$$

where $N = \langle \Psi_{\rm F}| \tilde{O}_{\rm L} \tilde{O}_{\rm R} |\Psi_{\rm I}\rangle$ is needed for the correct normalization. Note that the effective amplitude is intrinsically occupation-dependent.

As an example, for the conventional single-particle tunneling of bosons it follows $A^{\alpha,\beta} = -J_\alpha \delta_{\alpha,\beta}$ and $N = \sqrt{n_{\rm L}}\sqrt{n_{\rm R}+1}$. Here, $J_\alpha = -\langle w^{(\alpha)}| \frac{\mathbf{p}^2}{2m} + V(\mathbf{r}) |w^{(\alpha)}\rangle$ is the tunneling amplitude in band α. As another example, the multi-orbital bosonic bond-charge operator

$$\begin{aligned} \hat{X}_{\rm BB} = & \sum_{\{\alpha\},\{\beta\}} X_{\rm BB}^{\{\alpha\},\{\beta\}} \, \hat{b}_{\rm L}^{(\alpha_1)\dagger} \hat{b}_{\rm L}^{(\alpha_2)\dagger} \hat{b}_{\rm L}^{(\alpha_3)} \hat{b}_{\rm R}^{(\beta_1)} + \\ & \sum_{\{\alpha'\},\{\beta'\}} X_{\rm BB}^{\{\alpha'\},\{\beta'\}} \, \hat{b}_{\rm L}^{(\alpha_1')\dagger} \hat{b}_{\rm R}^{(\beta_1')\dagger} \hat{b}_{\rm R}^{(\beta_2')} \hat{b}_{\rm R}^{(\beta_3')} \end{aligned} \qquad (14)$$

decomposes in left and right part $\hat{O}_{\rm L}^{\{\alpha\}}$ and $\hat{O}_{\rm R}^{\{\beta\}}$, that consist of either one or three creation/annihilation operators. In contrast to the conventional tunneling, orbital-changing processes are allowed for the multi-orbital bond-charge operator.

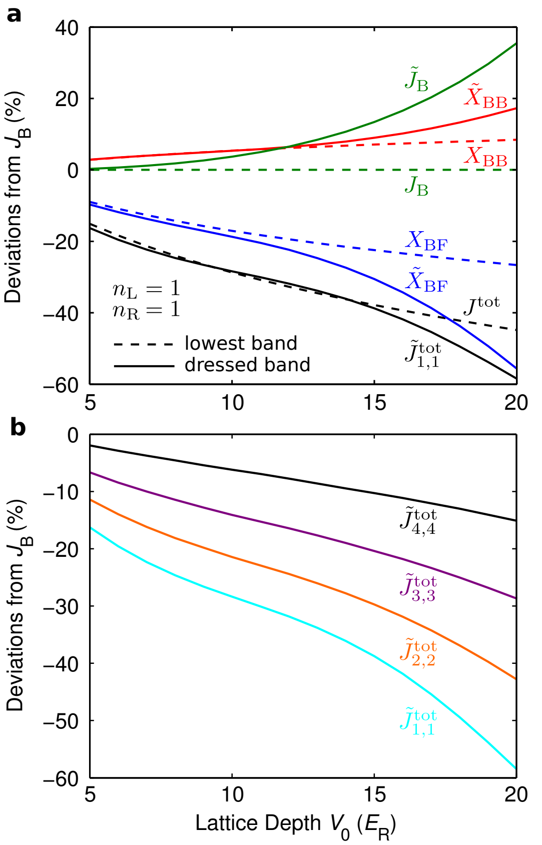

FIG. 4: **a** Contributions to the total tunneling in the lowest band (dashed) and the dressed band (solid) for one bosons and one fermion on each site. The total tunneling (black) is composed of conventional tunneling J (green), bosonic bond-charge tunneling X_BB (red), and fermionic bond-charge tunneling X_BF (blue). The absolute value of all matrix elements are enhanced by orbital degrees of freedom but due to their opposite signs the multi-orbital effects partly compensate each other. **b** Deviations of the total tunneling $\tilde{J}^\mathrm{tot}_{n,n} = \tilde{J}_\mathrm{B} + (n_\mathrm{L} + n_\mathrm{R} - 1)\tilde{X}_\mathrm{BB} + 2\tilde{X}_\mathrm{BF}$ from the standard Hubbard tunneling J_B for different bosonic occupations $n_\mathrm{L} = n_\mathrm{R}$.

The renormalized amplitudes are depicted in Fig. 4 for all relevant contributions to the total tunneling in the case of one boson and one fermion per site (solid lines). The amplitudes for conventional tunneling $\tilde{J}_{n_\mathrm{L},n_\mathrm{R}}$ (green line) as well as bond-charge induced tunneling $\tilde{X}_{\mathrm{BB},n_\mathrm{L},n_\mathrm{R}}$ (red) and $\tilde{X}_{\mathrm{BF},n_\mathrm{L},n_\mathrm{R}}$ (blue) can differ strongly from the lowest band values, which are indicated as dashed lines. The multi-orbital renormalization can enhance the conventional tunneling by up to 30% and the bond-charge induced processes can even be twice as strong as in the lowest single-particle band.

B. On-site problem and on-site interaction

This section is dedicated to the explicit solution of the many-body problem on a single lattice site for a given number of particles. For the multi-orbital dressing procedure (section III.A) we assume the ground state of the interacting system to be a product state of these solutions. We apply the method of exact diagonalization to compute the ground state $\Psi(n)$ of n bosons and one fermion on a single lattice site and thereby obtain the solution of the full lattice problem. In particular, this leads directly to an occupation-number-dependent on-site energy E_n. The respective single-site Hamiltonian reads

$$\begin{aligned}\hat{H}_\text{site} = &\sum_\alpha \epsilon_\mathrm{B}^{(\alpha)} \hat{n}^{(\alpha)} + \sum_\alpha \epsilon_\mathrm{F}^{(\alpha)} \hat{m}^{(\alpha)} \\ &+ \frac{1}{2} \sum_{\alpha\beta\gamma\delta} U_\mathrm{BB}^{(\alpha\beta\gamma\delta)}\, \hat{b}^{(\alpha)\dagger} \hat{b}^{(\beta)\dagger} \hat{b}^{(\gamma)} \hat{b}^{(\delta)} \\ &+ \sum_{\alpha\beta\gamma\delta} U_\mathrm{BF}^{(\alpha\beta\gamma\delta)}\, \hat{b}^{(\alpha)\dagger} \hat{f}^{(\beta)\dagger} \hat{f}^{(\gamma)} \hat{b}^{(\delta)},\end{aligned} \tag{15}$$

with the bosonic particle number operator $\hat{n}^{(\alpha)} = \hat{b}^{(\alpha)\dagger}\hat{b}^{(\alpha)}$ and the single-particle energies $\epsilon_\mathrm{B}^{(\alpha)}$. The operators $\hat{m}^{(\alpha)}$, $\hat{f}^{(\alpha)\dagger}$, $\hat{f}^{(\alpha)}$ and the energy $\epsilon_\mathrm{F}^{(\alpha)}$ are the fermionic analogues. The multi-band interaction amplitudes are defined as

$$\begin{aligned}U_\mathrm{BB/BF}^{(\alpha\beta\gamma\delta)} = g_\mathrm{BB/BF} \int \; & w_\mathrm{B}^{(\alpha)*}(\mathbf{r})\, w_\mathrm{B/F}^{(\beta)*}(\mathbf{r}')\, V(\mathbf{r},\mathbf{r}') \\ & \times w_\mathrm{B/F}^{(\gamma)}(\mathbf{r}')\, w_\mathrm{B}^{(\delta)}(\mathbf{r}) \;\; d^3r\, d^3r'.\end{aligned} \tag{16}$$

The interaction potential $V(\mathbf{r},\mathbf{r}')$ is a finite-range box potential with a width of 7.5 nm (see Ref. [17] for details). We expand this Hamiltonian in the basis of many-particle Fock-states $|N\rangle\,|M\rangle$. For n bosons and 1 fermion, the ground state is found by applying an exact diagonalization, the so-called configuration interaction method. We restrict the calculation to the lowest 9 bands per spatial direction and use a high energy cutoff [31]. The on-site energy is directly obtained as the lowest eigenvalue of the matrix and its contributions can be computed as expectation values of the individual operators in (15) using the corresponding eigenvector.

The energy contributions are plotted in Fig. 5**a** for $V_0 = 15\,E_\mathrm{R}$ and $n = 3$ bosons (solid lines). The values significantly deviate from the lowest-band approximation (dashed lines). The single-particle energies $n\tilde{\epsilon}_\mathrm{B} + \tilde{\epsilon}_\mathrm{F}$ (green line) are measured relative to the lowest-band values and thus are always positive. The occupation of higher orbitals causes a contraction of the wave functions which leads to an increase of the absolute value of the Bose-Fermi interaction. This results in a large reduction of the total on-site energy (black line) for large scattering lengths a_BF. Of course, also the repulsive interaction among the bosonic particles (red line) contributes but is less drastically influenced.

The total on-site energies for various boson numbers are shown in Fig. 5**b**. The dashed lines correspond to a calculation with a three times larger interaction range. In general, the contributions of higher bands are reduced with an increasing interaction range. The figure shows that the energy is only weakly affected by a the change of the (finite) interaction range. Additionally, we applied scaling theory to estimate the value of convergence for the on-site energy at the most demanding parameters $V_0 = 20\,E_\mathrm{R}$ and $a_\mathrm{BF} = -300\,a_0$ for an interaction range of 7.5 nm. We see that the error (differences in energies) converges exponentially with both the length of the many-particle basis and the number of orbitals. Scaling our results according to the exponential behavior, we are able to determine the converged energy value, where we first perform the scaling in respect to the basis length for a given number of orbitals. The results indicated as crosses in Fig. 5**b** show only small deviations and justify the constraints for the basis length and the number of orbitals applied for the solid lines.

The total on-site energy becomes intrinsically occupation-dependent (beyond the dependency in the standard Bose-Fermi Hubbard model (2)) and can be written in terms of effective n-particle collisions [18, 26, 27]

$$\tilde{E}_n = n\tilde{E}_1 + \frac{1}{2}n(n-1)\bar{E}_2 + \frac{1}{6}n(n-1)(n-2)\bar{E}_3 ... \quad (17)$$

The first term $\tilde{E}_1$ describes the interaction energy by two-particle collisions between bosons and fermions. The second term is the interaction energy caused by processes that involve two bosons $\bar{E}_2 = \tilde{E}_2 - 2\tilde{E}_1$ and the third term $\bar{E}_3 = \tilde{E}_3 - 3\bar{E}_2 - 3\tilde{E}_1$ involves three bosons. Although, the restriction to the first three terms is enough to describe well the energies for up to $n = 5$ bosons, we use here the exact values for $\tilde{E}_n$.

IV. SUPERFLUID TO MOTT-INSULATOR TRANSITION

After discussing off-site interactions and multi-orbital renormalizations, we now turn back to the full many-body quantum gas problem. Obviously, from the above results, it is necessary to take both bond-charge interactions and higher bands into account. First, we now define an extended model of the lowest band that includes off-site interactions and discuss its implications. Afterwards, we replace the lowest single-particle band and parameters with the respective dressed analogues and thereby include higher bands in a very efficient way.

The extended Hubbard model of the lowest band reads

$$\begin{aligned}\hat{H}_{\text{ext}} = & -\sum_{\langle i,j\rangle}\left[J_{\text{B}} + X_{\text{BB}}(\hat{n}_i + \hat{n}_j - 1) + 2\,X_{\text{BF}}\right]\hat{b}_i^\dagger \hat{b}_j \\ & + \frac{U_{\text{BB}}}{2}\sum_i \hat{n}_i(\hat{n}_i - 1) - \mu_{\text{eff}}\sum_i \hat{n}_i.\end{aligned} \quad (18)$$

While the repulsive interaction between the bosons increases the total tunneling, the attractive fermions reduce the bosonic mobility. As one central result and in strong contrast to the predictions of the standard Hubbard model (see section II) the superfluid to Mott-insulator transition is shifted. The phase diagrams are shown in Fig. 6 for different attractive Bose-Fermi interaction strengths. For strong Bose-Fermi attraction and low bosonic filling, the transition occurs at much shallower lattices, due to the effectively deepened tunneling-potential. The effect is reversed when the repulsion between the bosons becomes stronger than the attraction to the fermions, which is the case for weaker Bose-Fermi interaction and higher bosonic filling. In Fig. 1**b** the critical lattice depth for the transition is plotted as a function of the interspecies interaction strength a_{BF}. The dotted lines correspond to the extended Hamiltonian restricted to the lowest band.

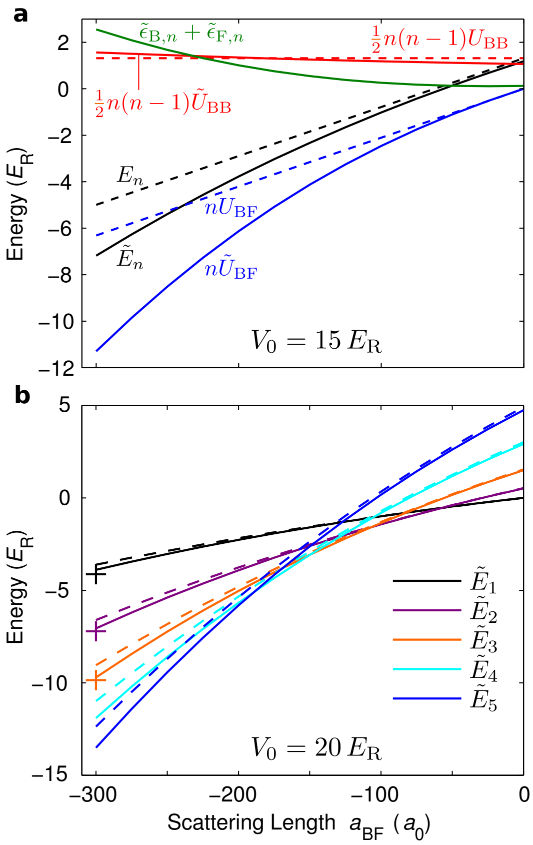

FIG. 5: **a** Total on-site energy E_n and its contributions for $n = 3$ bosons and $m = 1$ fermion as functions of the interspecies scattering length. The contributions are single-particle energies $\epsilon_{\text{B,F}}$ (green), Bose-Bose interaction U_{BB} (red), and Bose-Fermi interaction U_{BF} (blue). The total on-site energy is visibly lower than the lowest band prediction (dashed lines). **b** The total on-site energies E_n for various numbers of bosons n and one fermion. With increasing interspecies interaction the total energy decreases non-linearly. The dashed lines correspond to a three times larger interaction range. The markers are obtained by applying scaling theory as described in the text.

When including higher bands we must replace the lowest-band operators with those of the dressed band $\tilde{b}_i$ and $\tilde{b}_i^\dagger$. Also, the parameters J, X and U must be renormalized as discussed in section III. All tunneling contributions, i.e., conventional tunneling, both bond-charge interactions as well as their multi-orbital renormalizations can be combined to one total tunneling parameter

$$\tilde{J}^{\text{tot}}_{n_i,n_j} = \tilde{J}_{n_i,n_j} + \tilde{X}_{\text{BB},n_i,n_j}(n_i + n_j - 1) + 2\tilde{X}_{\text{BF},n_i,n_j}, \quad (19)$$

which is explicitly occupation-number dependent. The renormalized on-site energy

$$\tilde{E}_n = n\tilde{\epsilon}_{\text{B},n} + \tilde{\epsilon}_{\text{F},n} + \frac{1}{2}n(n-1)\tilde{U}_n + n\tilde{U}_{\text{BF},n} \quad (20)$$

is composed of the renormalized single particle energies of bosons $\tilde{\epsilon}_{\text{B},n}$ and fermions $\tilde{\epsilon}_{\text{F},n}$ as well as the interaction ener-

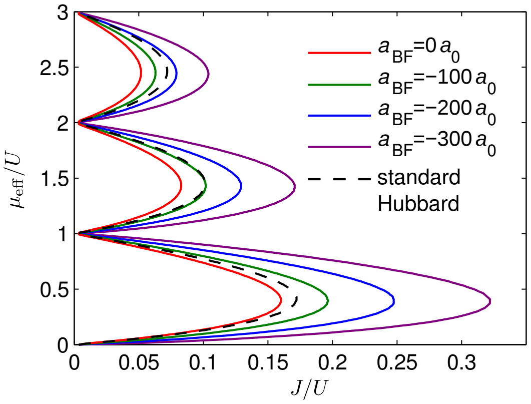

FIG. 6: Phase diagrams of the lowest-band model (18) with bond-charge interactions for different scattering lengths. For comparison the results of the standard Hubbard model are shown as a dashed black line.

gies for the repulsion between the bosons $\frac{1}{2}n(n-1)\tilde{U}_n$ and the attraction between the species $n\tilde{U}_{{\rm BF},n}$. This allows to define the extended Hamiltonian of the dressed band in equation (1), namely,

$$\tilde{H}_{\rm ext} = -\sum_{\langle i,j\rangle} \tilde{b}_i^\dagger \tilde{b}_j \tilde{J}^{\rm tot}_{\hat{n}_j,\hat{n}_i} + \sum_i \tilde{E}_{\hat{n}_i} - \mu \sum_i \hat{n}_i. \qquad (21)$$

The dressed-band Hamiltonian now takes into account all higher-band processes and all relevant nearest-neighbor interactions. The multi-orbital corrections of the Bose-Fermi interaction have a strong impact on the chemical potential at which the transition to a certain Mott-lobe occurs. This distorts and shifts the phase diagram along the axis of the chemical potential. Since this effect is not of any physical interest, we plot Fig. 1**a** in terms of an effective chemical potential $\mu_{\rm eff} = \mu - \tilde{E}_1$. Concerning the transition point of the bosonic superfluid to Mott-insulator transition, the reduction of the total on-site energy by multi-orbital processes counters the effect of reduced total tunneling. Nonetheless, the total effect on the transition can be a shift of several recoil energies $E_{\rm R}$ depending on interaction strengths and filling factors (Fig. 1**b**). Note that the lowest-band model $\hat{H}_{\rm ext}$ underestimates the impact on the superfluid to Mott-insulator transition by only up to $1E_{\rm R}$, which is surprising keeping the strong changes of the individual amplitudes in mind. However, this (coincidental) compensation of the contributing amplitudes depends on the choice of system parameters. Furthermore, it has been demonstrated that the on-site interaction [27, 30] and the effective tunneling matrix element [4] are experimentally well accessible and can be measured independently.

V. DENSITY-DENSITY INTERACTIONS AND PAIR-TUNNELING

In the above model, several off-site processes have been neglected due to their small amplitude in the lowest band. In this context the question arises, whether the multi-orbital dressing can enhance them to non-negligible values. The correlated pair tunneling and the density-density interactions both have very small amplitudes because in the integrand the small tail of the Wannier function enters quadratically on both lattice sites. By contrast, in the bond-charge integral the tail is multiplied three times with the center of a Wannier function. However, when taking into account strongly delocalized wave functions of higher bands, this argument no longer applies and all processes need to be reconsidered, since the overlap integrals become comparable for all types of off-site interactions. These contributions are strongly suppressed in the case of density-density interactions, because the initial and final state both depend on higher-band contributions with small coefficients $c_N \ll 1$ to produce a large integral, whereas in the case of pair tunneling one of them can be the ground state ($c_N \approx 1$). Although, the multi-orbitally renormalized pair tunneling is usually smaller than the conventional tunneling it can, in general, reach the same order of magnitude. Due to this structure it has very bad convergence properties in respect to the total number of contributing bands. As a fourth order contribution in perturbation theory it can, however, be neglected even for rather large amplitudes. Density-density interactions are not as strongly influenced and remain small. This justifies, the restriction to the extensions incorporated in Hamiltonian (1), which includes all relevant off-site interactions.

VI. CONCLUSIONS

We have discussed the important role of interaction effects in atomic quantum gas mixtures in optical lattices. Off-site interactions as well as higher band processes turn out to have a strong impact on these systems, which we are able to calculate using an extended occupation-dependent Hubbard model. In particular, we have focused on Bose-Fermi mixtures in this paper, where the standard Bose-Fermi-Hubbard model fails to cover all relevant processes. This manifests itself in a strong shift of the superfluid to Mott-insulator transition in the bosonic subsystem, which is not predicted by the standard Hubbard model. The critical lattice depth is shifted towards shallower lattices with increasing Bose-Fermi attraction. Similar corrections are present for all experiments with optical lattices and can be expected to be relevant, e.g., for Bose-Bose mixtures, low-dimensional systems or other lattice geometries. Omitting the condition of having a fermionic band insulator, which we have applied here, the presented extensions of the Bose-Fermi Hubbard model can lead to very rich physics such as the formation of polarons.

We have shown that for optical lattice systems the bond-charge tunneling [9, 12–18] is the most important contribution of the nearest-neighbor off-site interaction as it can drastically influence the tunneling. Repulsive interactions enhance the total tunneling, whereas the attractive interactions reduce it. In an intuitive picture, this can be described as lowered and increased effective potentials, respectively. Furthermore, higher band processes not only reduce the total on-site energy but also have an impact on the conventional tunneling and the bond-charge interactions. We have treated the problem by dressing [17, 18] the lowest single-particle band with interaction-induced occupations of higher-orbital states. This leads to a renormalization of interactions and tunneling parameters that become intrinsically occupation-dependent. These parameters have been used in order to define an extended Bose-Fermi-Hubbard model capable of describing effects of higher orbitals and off-site interactions in Bose-Fermi mixtures.

The results show in general that interactions in multi-component systems can have a crucial impact beyond the standard Hubbard treatment. In the presented case, the standard Hubbard model is incapable of describing the interspecies interaction between bosonic and fermionic atoms correctly. While here mainly the effects on the bosonic atoms have been discussed, the mutual interaction affects the fermionic atoms similarly, which has recently been observed in experiment [4].

VII. ACKNOWLEDGMENTS

We thank U. Bissbort and W. Hofstetter for stimulating discussions and acknowledge financial support by the German science foundation DFG under grant FOR801.

[1] K. Günter, T. Stöferle, H. Moritz, M. Köhl, and T. Esslinger, Phys. Rev. Lett. **96**, 180402 (2006).
[2] S. Ospelkaus, C. Ospelkaus, O. Wille, M. Succo, P. Ernst, K. Sengstock, and K. Bongs, Phys. Rev. Lett. **96**, 180403 (2006).
[3] T. Best, S. Will, U. Schneider, L. Hackermüller, D. van Oosten, I. Bloch, and D.-S. Lühmann, Phys. Rev. Lett. **102**, 030408 (2009).
[4] J. Heinze, S. Götze, J. S. Krauser, B. Hundt, N. Fläschner, D.-S. Lühmann, C. Becker, and K. Sengstock, Phys. Rev. Lett. **107**, 135303 (2011).
[5] M. Cramer, S. Ospelkaus, C. Ospelkaus, K. Bongs, K. Sengstock, and J. Eisert, Phys. Rev. Lett. **100**, 140409 (2008).
[6] M. Cramer, Phys. Rev. Lett. **106**, 215302 (2011).
[7] D.-S. Lühmann, K. Bongs, K. Sengstock, and D. Pfannkuche, Phys. Rev. Lett. **101**, 050402 (2008).
[8] R. M. Lutchyn, S. Tewari, and S. Das Sarma, Phys. Rev. A **79**, 011606 (2009).
[9] A. Mering and M. Fleischhauer, Phys. Rev. A **83**, 063630 (2011).
[10] A. Albus, F. Illuminati, and J. Eisert, Phys. Rev. A **68**, 023606 (2003).
[11] C. Kollath *et al.*, Phys. Rev. A **69**, 031601 (2004).
[12] J. E. Hirsch, Physica C **158**, 326 (1989).
[13] R. Strack and D. Vollhardt, Phys. Rev. Lett. **70**, 2637 (1993).
[14] J. E. Hirsch, Physica B **199/200**, 366 (1994).
[15] J. C. Amadon and J. E. Hirsch, Phys. Rev. B **54**, 6364 (1996).
[16] G. Mazzarella, S. M. Giampaolo, and F. Illuminati, Phys. Rev. A **73**, 013625 (2006).
[17] D.-S. Lühmann, O. Jürgensen, and K. Sengstock, New J. Phys. **14**, 033021 (2012).
[18] U. Bissbort, F. Deuretzbacher, and W. Hofstetter, arxiv:1108.6047v1 (2011).
[19] J. Li, Y. Yu, A. M. Dudarev, and Q. Niu, New J. Phys. **8**, 154 (2006).
[20] J. Larson, A. Collin, and J.-P. Martikainen, Phys. Rev. A **79**, 033603 (2009).
[21] K. R. A. Hazzard and E. J. Mueller, Phys. Rev. A **81**, 031602 (2010).
[22] O. Dutta, A. Eckardt, P. Hauke, B. Malomed, and M. Lewenstein, New J. Phys. **13**, 023019 (2011).
[23] K. Sakmann, A. I. Streltsov, O. E. Alon, and L. S. Cederbaum, Phys. Rev. Lett. **103**, 220601 (2009).
[24] K. Sakmann, A. I. Streltsov, O. E. Alon, and L. S. Cederbaum, Phys. Rev. A **82**, 013620 (2010).
[25] T. Busch, B.-G. Englert, K. Rząażewski, and M. Wilkens, Foundations of Physics **28**, 549 (1998).
[26] P. R. Johnson, E. Tiesinga, J. V. Porto, and C. J. Williams, New J. Phys. **11**, 093022 (2009).
[27] S. Will, T. Best, U. Schneider, L. Hackermüller, D.-S. Lühmann, and I. Bloch, Nature (London) **465**, 197 (2010).
[28] H. P. Büchler, Phys. Rev. Lett. **104**, 090402 (2010).
[29] S. Pilati and M. Troyer, arxiv:1108.1408 (2011).
[30] S. Will, T. Best, S. Braun, U. Schneider, and I. Bloch, Phys. Rev. Lett. **106**, 115305 (2011).
[31] The resulting many-body product basis has a total length of $12000n^2$, where n is the number of bosons.